Exosomes Derived From Schwann Cells Ameliorate Peripheral Neuropathy in Type 2 Diabetic Mice

Lei Wang,[1] Michael Chopp,[1,2] Alexandra Szalad,[1] XueRong Lu,[1] Yi Zhang,[1] Xinli Wang,[1] Pasquale Cepparulo,[1] Mei Lu,[3] Chao Li,[1] and Zheng Gang Zhang[1]

Diabetes 2020;69:749–759 | https://doi.org/10.2337/db19-0432

Schwann cell–derived exosomes communicate with dorsal root ganglia (DRG) neurons. The current study investigated the therapeutic effect of exosomes derived from healthy Schwann cells (SC-Exos) on diabetic peripheral neuropathy (DPN). We found that intravenous administration of SC-Exos to type 2 diabetic *db/db* mice with peripheral neuropathy remarkably ameliorated DPN by improving sciatic nerve conduction velocity and increasing thermal and mechanical sensitivity. These functional improvements were associated with the augmentation of epidermal nerve fibers and remyelination of sciatic nerves. Quantitative RT-PCR and Western blot analysis of sciatic nerve tissues showed that SC-Exo treatment reversed diabetes-reduced mature form of miRNA (miR)-21, -27a, and -146a and diabetes-increased semaphorin 6A (SEMA6A); Ras homolog gene family, member A (RhoA); phosphatase and tensin homolog (PTEN); and nuclear factor-κB (NF-κB). In vitro data showed that SC-Exos promoted neurite outgrowth of diabetic DRG neurons and migration of Schwann cells challenged by high glucose. Collectively, these novel data provide evidence that SC-Exos have a therapeutic effect on DPN in mice and suggest that SC-Exo modulation of miRs contributes to this therapy.

Peripheral neuropathy is the most prevalent complication of diabetes, and clinical symptoms originate from distal sensory nerves. Diabetic peripheral neuropathy (DPN) has a complex pathogenesis and is associated with axonal degeneration and segmental demyelination. Current treatment options for DPN are meager (1–3).

Myelin-forming Schwann cells, the most abundant cells in the peripheral nervous system, interact with axons and blood vessels to regulate peripheral nerve function (1,4,5). Dysfunction of these interactions contributes to the development of DPN (6,7). Alteration of mature form of miRNA (miR) expression provokes diabetic neuropathy (8–10). Patients with type 2 diabetes (T2D) exhibit increased susceptibility to neuropathy when they have polymorphisms in miR-146a, miR-27a, and miR-124a genes (11). Treatment of diabetic mice with miR-146a mimics reduces DPN by targeting proinflammatory genes, interleukin-1 receptor–associated kinase (IRAK1), and tumor necrosis factor receptor–associated factor 6 (TRAF6) (12). A recent study in type 1 diabetic mice with DPN showed that these mice exhibit significantly reduced levels of let-7i and miR-27a, among other miRs (13). Intranasal administration of exogenous let-7i miRNA substantially decreases DPN (14).

Exosomes are nanovesicles (30–200 nm) and play a major role in mediating intercellular communication through transferring their bioactive cargo, including miRs, to recipient cells, ultimately regulating recipient cell function (15,16). We previously demonstrated that exosomes derived from high-glucose (HG)–challenged Schwann cells promote the development of DPN in T2D mice (17), while others have shown that exosomes derived from healthy Schwann cells (SC-Exos) substantially enhance regeneration of injured peripheral axons in a rat model of sciatic nerve injury (18). However, the therapeutic effect of SC-Exos on DPN has not been investigated. Here, we report that treatment of T2D mice with SC-Exos robustly ameliorates DPN by reducing peripheral nerve damage.

RESEARCH DESIGN AND METHODS

All experimental procedures were approved by the institutional animal care and use committee of Henry Ford

[1]Department of Neurology, Henry Ford Hospital, Detroit, MI
[2]Department of Physics, Oakland University, Rochester, MI
[3]Department of Biostatistics and Research Epidemiology, Henry Ford Hospital, Detroit, MI

Corresponding author: Lei Wang, leiwang@neuro.hfh.edu

Received 29 April 2019 and accepted 31 December 2019

This article contains Supplementary Data online at https://diabetes.diabetesjournals.org/lookup/suppl/doi:10.2337/db19-0432/-/DC1.

Hospital (IACUC #1656) and were performed according to National Institutes of Health Guidelines for the Care and Use of Laboratory Animals. Male BKS.Cg-$m^{+/+}Lepr^{db}/J$ (*db/db*) and heterozygote mice (*db/m*, a nonpenetrant genotype; The Jackson Laboratory) at the age of 20 weeks were used. All procedures and analyses were performed by investigators who were blinded to the administered treatment.

Generation and Characterization of SC-Exos and Fibroblast Cell Exosomes

Primary Schwann cells isolated from neonatal C57BL/6 mouse sciatic nerves were well characterized morphologically and phenotypically (S100, GFAP, and $CD9^+$) and were cultured in Schwann cell medium (ScienCell). Fibroblast cells were isolated from mouse subcutaneous tissue and cultured in DMEM (ATCC). For the exosome isolation, culture medium was replaced with 5% exosome-depleted FBS-containing medium (System Biosciences) when they reach 60–80% confluence, and the cells were cultured for an additional 48 h. The supernatant was collected to extract exosomes using a differential ultracentrifugation approach. Briefly, the supernatant was filtered through a 0.22-μm filter and subjected to centrifugation at 10,000*g* for 30 min. Ultracentrifugation was then performed at 100,000*g* for 3 h, and the pellet was resuspended with 100 μL of sterilized PBS. The number and size of exosomes were quantified using the NanoSight analysis system (Malvern Panalytical). Transmission electron microscopy (TEM) and Western blot analysis with antibodies against exosome proteins, Alix, CD63, and HSP70 were performed to further confirm exosomes (17,19–21).

To track tissue distribution of SC-Exos, we generated SC-Exos carrying CD63-GFP (SC-Exos-GFP). Briefly, Schwann cells were transfected with a pEGFP vector carrying EGFP-fused CD63 gene (Plasmid #62964; Addgene) through electroporation using the Nucleofector kit (Lonza). SC-Exos-GFP were isolated from the supernatant of transfected cells.

Liposome Preparation

To mimic the exosomal lipid layer, we generated liposomes that contained three major fatty acids present in exosomes using the thin-film hydration technique (22). Details are provided in the Supplementary Material.

To examine whether miR-27a contributes to the effect of SC-Exos on neurite outgrowth and Schwann cell migration, we generated SC-Exos with reduced miR-27a. Briefly, Schwann cells were transfected with an miR-27a inhibitor (mmu-miR-27a-3p, miRCURY LNA miR inhibitor; Exiqon) or a scrambled control (miRCURY LNA miR inhibitor control; Exiqon) using electroporation (17). Exosomes were isolated as aforementioned. Quantitative PCR was performed to verify the transfection efficiency.

In Vivo Experimental Protocols

Male diabetic *db/db* mice and nondiabetic *db/m* mice at the age of 20 weeks were randomly divided into the following treatment groups: *1*) *db/m* + saline ($n = 15$), *2*) *db/db* + saline ($n = 15$), *3*) *db/db* + SC-Exos ($n = 15$), *4*) *db/db* + fibroblast cell exosomes (FC-Exos) ($n = 8$), and *5*) *db/db* + liposome ($n = 8$). SC-Exos, FC-Exos, and liposomes (4×10^{10} particles in 0.2 mL PBS/mouse) or an equal volume of saline were intravenously administered through a tail vein once every 2 weeks for 8 consecutive weeks. All mice were sacrificed 8 weeks after the initial treatment. The doses of exosomes were selected on the basis of published studies (23).

To examine whether SC-Exos intravenously administered are internalized by sciatic nerve fibers, SC-Exos-GFP (4×10^{10} particles/mouse) were intravenously injected into *db/db* mice ($n = 3$), and *db/db* mice ($n = 3$) that received naive SC-Exos were used as a control. Four hours after the injection, the mice were sacrificed. Sciatic nerves were harvested and teased into individual nerve fibers on glass slides for immunofluorescent staining.

Additionally, immunogold staining was performed to detect GFP-positive particles at ultrastructural levels using TEM. Briefly, sciatic nerves were fixed by 2.5% glutaraldehyde in 0.1 mol/L sodium cacodylate buffer for 24 h at 4°C. The nerves were postfixed by 1% osmium tetroxide/1.5% potassium ferrocyanide for 1 h at room temperature. The nerves were then embedded into resin mixture. The ultrathin sections (85 nm) were cut and mounted on nickel grids. Immunogold staining was performed with 2% anti-GFP rabbit monoclonal antibody (G10362; Thermo Fisher Scientific) and 10-nm Gold particle-conjugated streptavidin (25269; Electron Microscopy Sciences). The grids were imaged under TEM (EM208; Phillips).

Electrophysiological measurements and functional tests were performed before the treatment as a baseline and then every 2 weeks and 4 weeks, respectively.

In Vitro Experimental Protocols

Dorsal root ganglia (DRG) neurons were isolated from 20-week-old *db/m* and *db/db* mice and cultured under regular-glucose (RG) (5 mmol/L) and high-glucose (HG) (30 mmol/L) conditions. To assess the effect of SC-Exos on neurite outgrowth, DRG neurons were treated with *1*) *db/m* + RG, *2*) *db/db* + HG, *3*) *db/db* + HG + SC-Exos, *4*) *db/db* + HG + SC-Exos with reduced miR-27a (miR-27^{si}Exos), and *5*) *db/db* + HG + SC-Exo with scrambled control. Exosomes at a concentration of 6×10^9 particles/mL were used.

To track the internalization of SC-Exos in vitro, SC-Exos were transfected with Texas Red–labeled siRNA using an Exo-fect Exosome Transfection Kit (System Biosciences). Briefly, 3×10^{11} SC-Exos were incubated with transfection solution and siRNA at 37°C for 10 min, and then SC-Exos were placed on ice for 30 min to stop the reaction. Transfected SC-Exos were harvested by 13,000 rpm centrifugation for 30 min and immediately incubated with DRG neurons for 24 h. DRG neurons were stained with antibody against microtubule-associated protein 2 (MAP2, 1:500; Abcam) (20).

To assess the effect of SC-Exos on Schwann cells, Schwann cells were treated with *1*) RG, *2*) HG, *3*) HG + SC-Exos, *4*)

HG + SC-Exos with miR-27^{si}Exos, and 5) HG + SC-Exo with scrambled control. Exosomes at a concentration of 6×10^9 particles/mL were used.

Electrophysiological Measurements

Motor nerve conduction velocity (MCV) and sensory nerve conduction velocity (SCV) in sciatic nerve were measured with orthodromic recording techniques (24). MCV and SCV were calculated in accordance with published studies (24–26).

Measurement of Thermal Sensitivity

Plantar tests (Hargreaves method) were conducted using a thermal stimulation meter (Model 336 TG; IITC Life Science), as previously described (25,26).

Measurement of Mechanical Sensitivity

A series of von Frey filaments (Stoelting) were used to stimulate the plantar surface of the left hind paw with a pressure causing the filament to buckle. Paw withdrawal in response to each stimulus was recorded, and a 50% paw withdrawal threshold was calculated using a published equation (26–28).

Biochemical and Lipid Analyses

Levels of blood glucose were measured using an instant check meter (Roche Diagnostics) every 2 weeks. HbA_{1c} was measured with A1CNow+ Multi-Test A1C System before the treatment and at the end of the experiment. The levels of triglycerides and total cholesterol in plasma and liver tissues were measured with Triglyceride and Cholesterol Assay Kits (Abcam) at the end of the experiment.

Immunohistochemistry and Image Quantification

For analysis of intraepidermal nerve fiber (IENFs), footpad tissue cryosections (20 μm thick) stained with antibody against protein gene product 9.5 (PGP9.5, 1:1,000; Millipore) were imaged under a 40× objective (Carl Zeiss). Image analysis was performed using the MicroComputer Imaging Device (MCID) imaging system (Imaging Research Inc.). The number of nerve fibers crossing the dermal-epidermal junction were measured, and interepidermal nerve fiber density was presented as the number of fibers per millimeter of length of epidermis. Representative images of IENFs were captured with a laser scanning confocal microscope (Olympus Corporation) (25,26).

For analysis of morphometric changes of sciatic nerve, nerve samples were processed, respectively, as previously reported (25,29,30). The semithin transverse sections (2 μm thick) of sciatic nerve stained with toluidine blue were randomly imaged using a 100× oil immersion lens (Olympus Optical Co., Ltd.). Myelin sheath thickness, myelinated fiber, and axon diameter were measured using the MCID system, as previously reported (25,26). Ultrastructure myelination and axons were analyzed by TEM (30).

MiR fluorescence in situ hybridization combined with immunohistochemical staining were conducted as previously described (31). Briefly, the sections were hybridized with miR-27a LNA probe (Exiqon), and the probe was detected using peroxidase-conjugated anti-FAM (Roche). The sections were incubated with tyramide signal amplification substrate. Primary antibody neurofilament 200 (1:500; Sigma) was incubated and detected with FITC-conjugated secondary antibody (Jackson ImmunoResearch).

Measurement of Neurite Outgrowth

DRG neurons (2,000 cell/cm^2) were seeded on glass coverslips coated with poly-D-lysine and laminin in neurobasal-A

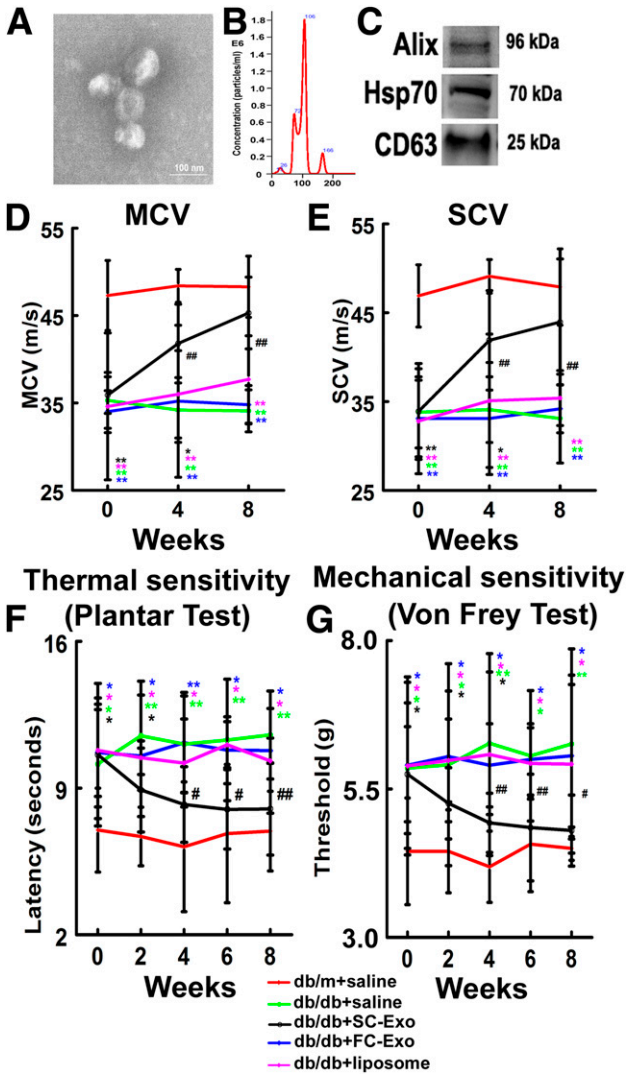

Figure 1—SC-Exos improve neurological function in *db/db* mice. SC-Exos characterized by TEM (*A*), NanoSight (*B*), and Western blot analysis (*C*). Treatment of diabetic mice with SC-Exos (db/db+SC-Exo, black, $n = 10$ mice/group), but no FC-Exos (db/db+FC-Exo, blue, $n = 8$ mice/group) and liposome (db/db+liposome, purple, $n = 8$ mice/group), improves neurological function measured by MCV (*D*), SCV (*E*), plantar test (*F*), and von Frey test (*G*), respectively. Scale bar = 100 nm. $^*P < 0.05$, $^{**}P < 0.01$ vs. the nondiabetic mice treated with saline (db/m+saline, red, $n = 10$ mice/group); $\#P < 0.05$, $\#\#P < 0.01$ vs. the diabetic mice treated with saline (db/db+saline, green, $n = 10$ mice/group).

Table 1—Effect of SC-Exos on body weight, blood glucose, and HbA_{1c}

Group	0 weeks	2 weeks	4 weeks	6 weeks	8 weeks
Body weight (g)					
db/m + saline	30.4 ± 1.26	31.3 ± 1.63	32.1 ± 1.91	31.6 ± 2.31	31.6 ± 1.26
db/db + saline	54.4 ± 1.71*	52.2 ± 4.36*	50.2 ± 5.00*	50.2 ± 3.25*	50.8 ± 3.66*
db/db + SC-Exo	50.0 ± 10.4*	53.4 ± 3.27*	52.4 ± 3.68*	50.7 ± 3.86*	51.1 ± 4.59*
db/db + FC-Exo	53.9 ± 4.15*	54.2 ± 3.86*	49.0 ± 5.52*	50.3 ± 7.9*	49.3 ± 6.18*
db/db + liposome	55.1 ± 4.45*	54.4 ± 4.11*	50.1 ± 4.63*	52.4 ± 3.86*	48.0 ± 5.8*
Blood glucose (mg/dL)					
db/m + saline	133 ± 24.0	142 ± 15.2	128 ± 8.56	122 ± 10.1	139 ± 12.89
db/db + saline	448 ± 51.6*	450 ± 96.7*	529 ± 38.6*	550 ± 38.3*	513 ± 26.7*
db/db + SC-Exo	429 ± 75.2*	462 ± 83.6	503 ± 32.3*	537 ± 32.7*	515 ± 42.1*
db/db + FC-Exo	503 ± 32.8*	499 ± 43.8*	514 ± 9.3*	520 ± 55.6*	519 ± 49*
db/db + liposome	491 ± 51.3*	506 ± 37.3*	502 ± 16.8*	508 ± 15.9*	514 ± 35.9*

	0 weeks		8 weeks	
HbA_{1c}	%	mmol/mol	%	mmol/mol
db/m + saline	4.3 ± 0.37	23.9 ± 4.1	4.4 ± 0.35	24.9 ± 4.0
db/db + saline	9.9 ± 1.76*	85.4 ± 19.3	10.4 ± 0.84*	90.7 ± 9.1
db/db + SC-Exo	10.4 ± 1.99*	90.2 ± 22.1	10.1 ± 1.29*	87.4 ± 14.9
db/db + FC-Exo	10.7 ± 0.75*	94.2 ± 8.3	10.1 ± 1.5*	87.0 ± 16.2
db/db + liposome	10.7 ± 1.53*	94.3 ± 16.8	10.5 ± 0.83*	91.6 ± 9.3

db/m, *db/db*, and *db/db* + SC-Exo, $n = 10$ mice/group. *db/db* + FC-Exo and *db/db* + liposome, $n = 8$ mice/group. 0 weeks, before treatment. *$P < 0.01$ vs. *db/m* + saline group.

medium containing 2% B-27 (Invitrogen). After a 3-day culture, DRG neurons were stained with antibody against neurofilament heavy subunit (1:500; BioLegend). The images were obtained using 10× magnification with a digital camera. The total neurite lengths of each neuron of 20 neurons per group were analyzed with the MCID system. The average length of neurite outgrowth was calculated (26).

Cell Migration Assay

Schwann cells were grown to a 90% confluent monolayer in six-well culture dishes under RG (5 mmol/L) and HG (30 mmol/L) conditions. A scratch wound was made with a 10-μL pipette tip. After 20 h of growth, images were taken, and the scratched gap distance of each image was quantified using the MCID system (32).

Quantitative Real-time RT-PCR Analysis

Total RNA was isolated by RNeasy Mini Kit (QIAGEN). Quantitative real-time RT-PCR (qRT-PCR) was performed according to published methods (12,17). The primers used are provided in Supplementary Table 1.

Western Blot Analysis

Western blot analysis was performed according to published protocols (17,25). The antibodies used are given in Supplementary Table 2.

Bioinformatics Analysis

Ingenuity Pathways Analysis (IPA) software (QIAGEN) was used to analyze signaling pathways and to a generate network graph of miRs and their related proteins.

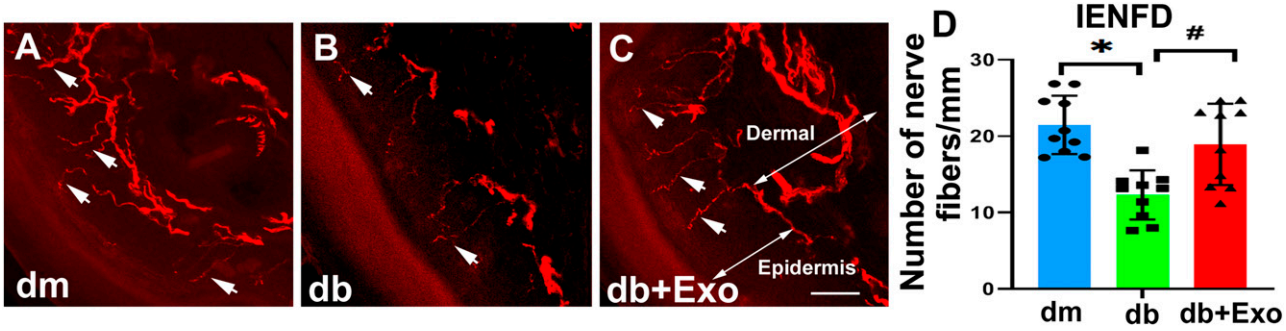

Figure 2—SC-Exos increase IENF density (IENFD). Representative images show PGP9.5-immunoreactive IENFs (red, arrows) in the hind plantar paw skin from nondiabetic mice (dm) (*A*), diabetic mice treated with saline (db) (*B*), and diabetic mice treated with SC-Exos (db+Exo) (*C*). Histogram represents the quantitative data of the IENFD under various conditions (*D*). Scale bar = 50 μm. $n = 10$ mice/group. *$P < 0.05$ vs. dm mice treated with saline; #$P < 0.05$ vs. db mice treated with saline.

Statistical Analysis

Data were evaluated for normality. The generalized estimating equation global test was used to analyze the effects of SC-Exo treatment on nerve conduction velocities (NCVs). Repeated-measures ANOVA (ANCOVA) was used to analyze the treatment effect in individual NCV, plantar test, and von Frey test over time. The analysis started testing for group-by-time interaction followed by testing for the main effect of group and subgroup analyses. One-way ANOVA followed by Tukey test was used for multiple group comparisons. Student *t* test was performed for two-group comparisons. Data are presented as mean ± SD. Statistical significance was detected at $P < 0.05$.

Data and Resource Availability

The data sets and resource generated and/or analyzed during the current study are available from the corresponding author upon reasonable request.

RESULTS

SC-Exos Improve Neurological Function in Mice With DPN

Using a differential ultracentrifugation approach, we isolated exosomes from the supernatant of Schwann cells cultured with exosome-depleted medium. TEM and NanoSight analysis revealed that SC-Exos had an average size of 102.3 ± 11.4 nm, and these exosomes exhibited the exosomal marker proteins Alix, HSP70, and CD63 (Fig. 1).

We then treated the *db/db* mice with SC-Exos at a dose of 4×10^{10} particles/mouse/injection through a tail vein starting at the age of 20 weeks when these mice developed DPN. Compared with *db/db* mice treated with saline, *db/db* mice treated with SC-Exos exhibited significantly improved MCV and SCV in the sciatic nerve, thermal latency (plantar test), and mechanical latency (von Frey test) starting at 4 weeks, which were maintained during the 8 weeks of treatment (Fig. 1). The effect of the SC-Exos on DPN is specific because FC-Exos did not improve NCVs and the mechanical and thermal sensitivity (Fig. 1). Moreover, treatment of *db/db* mice with liposome mimics containing lipid components did not show significant improvement of functional outcome compared with saline treatment (Fig. 1). The SC-Exo treatment did not significantly alter blood glucose levels, HbA_{1c}, and animal body weight compared with the saline treatment (Table 1). Additionally, *db/db* mice had increased levels of triglyceride and total cholesterol in plasma and liver compared with *db/m* mice. SC-Exos did not significantly reduce triglyceride levels of *db/db* mice, although SC-Exos reduced mean levels of triglyceride. Total cholesterol levels in SC-Exos–treated *db/db* mice were not different from control *db/db* mice (Supplementary Table 3). Collectively, these data demonstrate that treatment with SC-Exos ameliorates DPN.

SC-Exos Reduce Diabetes-Induced Sciatic Nerve Damage

Immunostaining analysis of the footpad tissues of mice at age 28 weeks showed that compared with nondiabetic

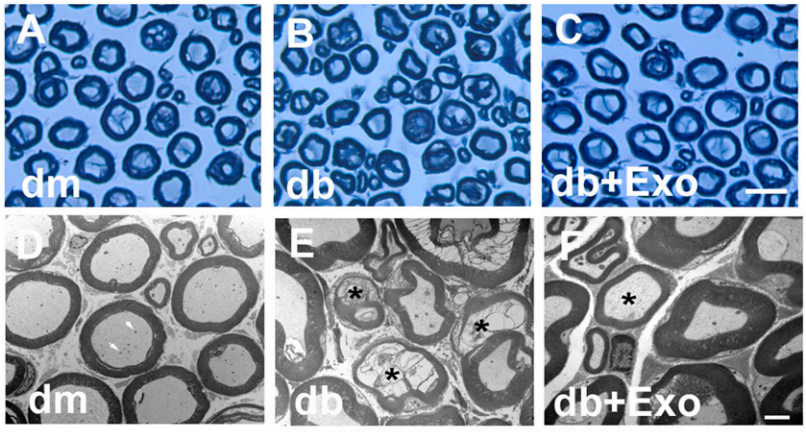

Effect of SC-Exos on histomorphometric parameters of sciatic nerves

Property	dm	db	db+Exo
Fiber diameter(μm)	8.84±0.42	7.68±0.30**	8.88±0.46##
Axon diameter(μm)	5.21±0.30	4.79±0.25**	5.20±0.28#
Myelin thickness(μm)	1.82±0.10	1.44±0.06**	1.83±0.1##
G ratio	0.59±0.01**	0.62±0.01**	0.58±0.02##

**p<0.01 versus dm-saline group and #p<0.05, ##p<0.01 versus db-saline group. n=10/group.

Figure 3—Effect of SC-Exos on histomorphometric changes of sciatic nerves. Representative images of semithin toluidine blue–stained cross sections of sciatic nerves from nondiabetic mice (dm) (*A*), diabetic mice treated with saline (db) (*B*), and diabetic mice treated with SC-Exos (db + Exo) (*C*). TEM images of ultrastructure of sciatic nerve from dm (*D*), db (*E*), db + Exo (*F*) mice. Intact myelinated axons with few mitochondria (arrows) in a dm mouse (*D*). Demyelinated and damaged axons (asterisks) in a db mouse (*E*). Axon with thin myelin (asterisk) in a db + Exo mouse, indicating remyelination (*F*). The table shows the quantitative data of a histomorphometric parameter of toluidine blue–stained sciatic nerve. Scale bars = 25 μm (*C*) and 1 μm (*F*).

db/m mice, *db/db* mice exhibited a significant reduction of PGP9.5-positive sensory IENF density, whereas the SC-Exo treatment significantly increased IENF density in *db/db* mice compared with the saline treatment (Fig. 2). In contrast, FC-Exos did not significantly increase IENF density in *db/db* mice (Supplementary Fig. 1). Moreover, analysis of toluidine blue–stained sciatic nerves showed that *db/db* mice exhibited substantial reduction of sciatic nerve fiber diameter and myelin sheath thickness and an increase in g-ratio (axon diameter/fiber diameter). However, SC-Exo treatment significantly reduced the sciatic nerve morphology altered by diabetes. Additional ultrastructural analysis of sciatic nerves showed robust reduction of demyelination and axonal damage and augmentation of remyelination in *db/db* mice treated with SC-Exos (Fig. 3).

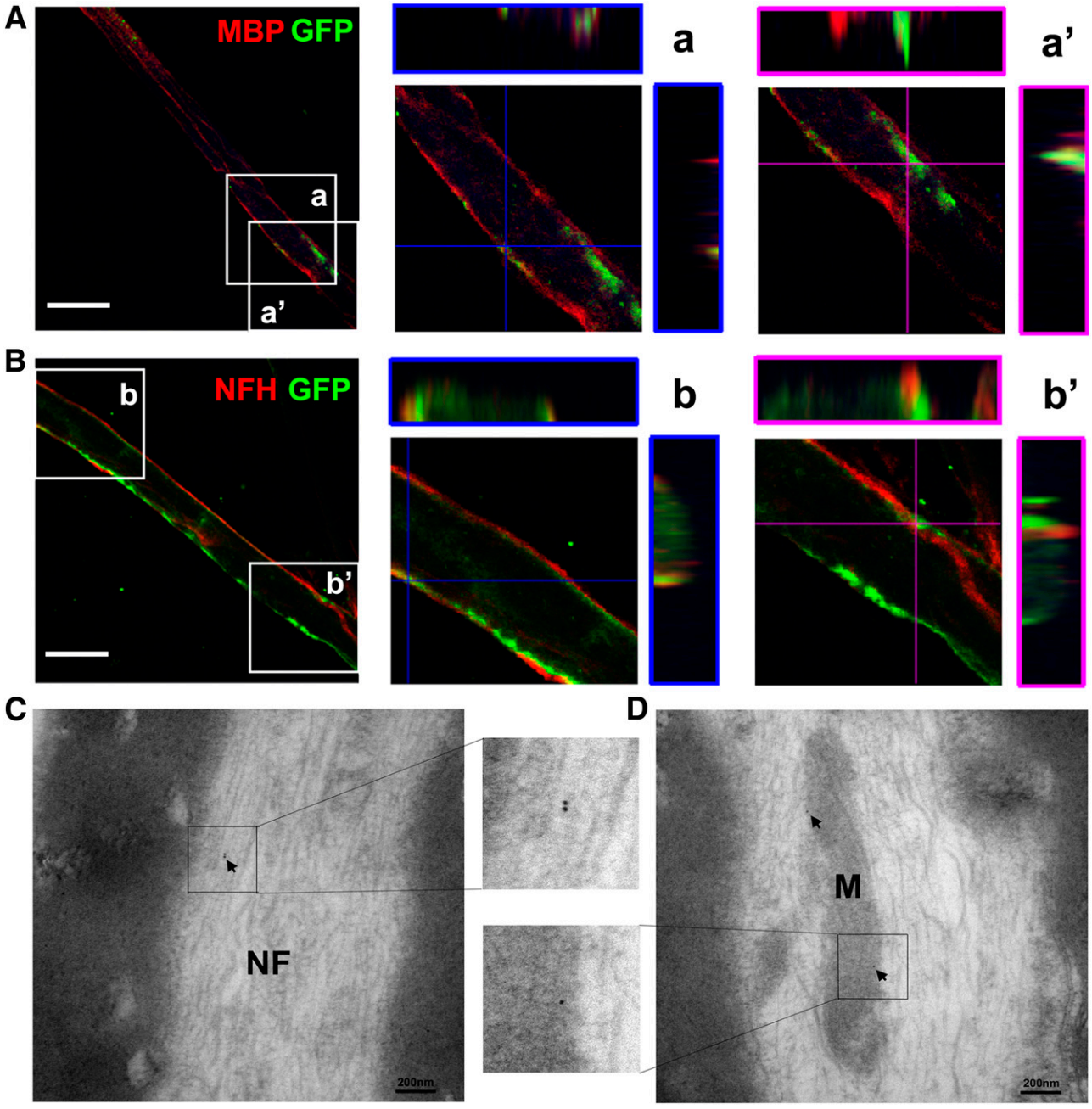

Figure 4—Distribution of SC-Exos in the sciatic nerve tissue. Representative confocal microscopic images show that these nerve fibers are MBP positive (red) (*A*) and NFH positive (red) (*B*) with the presence of puncta GFP (green) signals. The orthographic three-dimensional projection in enlarged areas demonstrated that GFP signals are colocalized to MBP (*a*) and NFH (*b*). However, some of GFP signals are localized within the MBP-positive signals (*a'*) and outside the NFH-positive signals (*b'*). These data suggest that SC-Exos-GFP are internalized by MBP-positive Schwann cells and NFH-positive nerve fibers of the sciatic nerve. TEM images show that GFP immunogold-positive particles (arrows) are present in the neurofilament (NF) (*C*) and mitochondria (M) (*D*) of sciatic nerves, indicating the presence of SC-Exos-GFP in nerve fibers of the sciatic nerve. $n = 3$ mice/group. Scale bars = 20 μm (*A* and *B*).

To examine whether administered SC-Exos reach to sciatic nerves, SC-Exos-GFP were intravenously administered to *db/db* mice. Three-dimensional confocal image analysis of double immunofluorescently stained sciatic nerves showed that GFP signals were colocalized to MBP-positive cells and neurofilament H (NFH)–positive nerve fibers (Fig. 4). TEM images showed that GFP immunogold-positive particles were detected in neurofilaments and mitochondria of sciatic nerves (Fig. 4). Taken together, our results demonstrate that SC-Exos are internalized by Schwann cells and nerve fibers.

SC-Exo Treatment Reverses Diabetes-Altered miRs and Proteins in the Sciatic Nerve

We and others have demonstrated that miRs are involved in the progression of diabetes and DPN (8–10). qRT-PCR analysis showed that DPN significantly reduced many miRs in sciatic nerve tissues compared with sciatic nerve tissue in *db/m* mice (Fig. 5). Substantially reduced miRs included miR-21, -27a, and -146a, which are consistent with findings from studies in patients and experimental animals with diabetes (12,14,33). The SC-Exo treatment significantly increased miR-21, -27a, and -146a in sciatic nerve tissues (Fig. 5), whereas treatment of *db/db* mice with FC-Exos did not significantly alter miR-21, -27a, and -146a levels (Supplementary Fig. 1). In situ hybridization analysis with LNA probes specific to mature miR-27a revealed that NF-200–positive DRG neurons in *db/m* mice expressed abundant miR-27a, while DRG neurons from *db/db* mice exhibited substantial reduction of miR-27a. The SC-Exo treatment considerably overcame diabetes-reduced miR-27a signals in DRG neurons in *db/db* mice (Fig. 5). We then analyzed these miRs in SC-Exos and found that compared with the FC-Exos, miR-21, -27a, and -146a were enriched in the SC-Exos (Fig. 5), suggesting that SC-Exos may transfer these miRs into sciatic nerve tissues. Furthermore, Western blot analysis of sciatic nerve tissues showed that the DPN considerably increased semaphorin 6A (SEMA6A); Ras homolog gene family, member A (RhoA); phosphatase and tensin homolog (PTEN); and phosphorylated nuclear factor-κB (pNF-κB), whereas the SC-Exo treatment, but not FC-Exos, significantly reduced SEMA6A, RhoA, PTEN, and pNF-κB compared with the saline treatment (Fig. 5 and Supplementary Fig. 1). Using bioinformatics analysis with IPA, we found that SEMA6A, RhoA, and PTEN are among genes putatively targeted by miR-21, -27a, and -146a, respectively, while NF-κB is an indirect target (Fig. 5). Upregulation of SEMA6A, RhoA, PTEN, and NF-κB induces peripheral nerve dysfunction (34–38). Thus, an inverse association between these miRs and the proteins SEMA6A, RhoA, PTEN, and NF-κB suggest that miR-21, -27a, and -146a transferred by SC-Exos potentially target SEMA6A, RhoA, PTEN, and NF-κB proteins in the sciatic nerve tissues, which may contribute to improved peripheral nerve function.

SC-Exos Promote Neurite Outgrowth of DRG Neurons and Migration of Schwann Cells In Vitro

To examine the direct effect of SC-Exos on axonal growth of DRG neurons, we performed in vitro experiments. DRG neurons harvested from *db/db* mice exhibited substantially reduced neurite outgrowth compared with DRG neurons

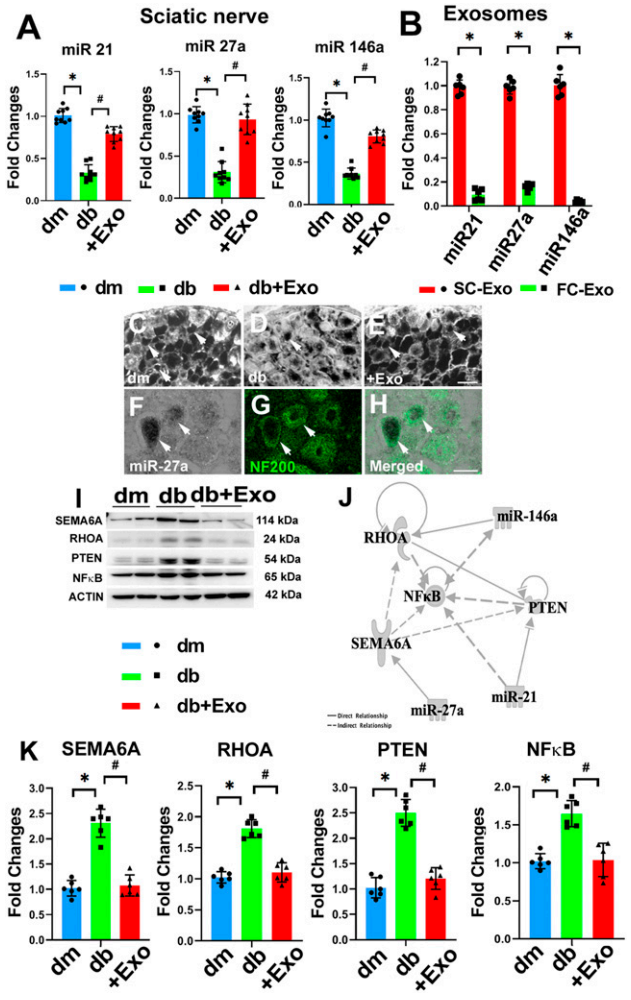

Figure 5—SC-Exos increase miR-21, -27a, and -146a and decrease SEMA6A, RhoA, PTEN, and pNF-κB proteins in the sciatic nerve tissue. qRT-PCR data of miR-21, -27a, and -146a levels in sciatic nerve tissue in nondiabetic mice (dm), diabetic mice treated with saline (db), and diabetic mice treated with SC-Exos (db + Exo) (n = 9 mice/group) (*A*). Profiles of miR-21, -27a, and -146a in SC-Exos and FC-Exos (n = 6/group) (*B*). Representative images of in situ hybridization with LNA miR-27a probes showing miR-27a signals (arrow) in cytoplasm of DRG neurons of dm mice (*C*) and db (*D*) or SC-Exos (+Exo) (*E*) mice. miR-27a signals had the same pattern in the three individual mice per group. Representative images of miR-27a signals colocalized with NF-200–positive DRG neurons (n = 3 mice/group) (*F–H*). Scale bars = 20 μm. Representative Western blot image (*I*) and quantitative data (*K*) of protein levels of SEMA6A, RhoA, PTEN, and pNF-κB in sciatic nerve tissues of dm, db, and db + Exo mice (n = 6 mice/group). Fold changes normalized to control. Signaling network of miR-21, -27a, and -146a and their related proteins (target genes), which was generated using IPA pathway building tools (*J*). *P < 0.05 vs. dm mice; #P < 0.05 vs. db mice.

from *db/m* mice (Fig. 6). However, the addition of SC-Exos (6×10^9 particles/mL) into diabetic DRG neurons completely reversed the diabetes-reduced neurite growth. Confocal microscopic analysis showed that Texas Red–labeled SC-Exos were internalized by MAP2-positive DRG neurons (Fig. 6). To examine the cause-effect of miR-27a within SC-Exo cargo on neurite outgrowth, we generated SC-Exos carrying reduced miR-27a (miR-27^{si}Exos). qRT-PCR analysis revealed that compared with SC-Exos derived from scrambled siRNA-transfected cells, levels of miR-27a within miR-27^{si}Exos were reduced by 51%. Treatment of diabetic DRG neurons with miR-27a^{si}Exos did not significantly promote neurite outgrowth. In addition to DRG neurons, naive SC-Exos abolished HG-inhibited Schwann cell migration, whereas miR-27a^{si}Exos did not suppress HG-reduced Schwann cell migration (Fig. 7). These in vitro data suggest that SC-Exos are internalized by DRG axons and facilitate neurite growth of diabetic DRG neurons and migration of Schwann cells and that SC-Exo cargo miR-27a contributes to SC-Exos–increased neurite outgrowth in diabetic DRG neurons and Schwann cell migration.

DISCUSSION

The current study for the first time demonstrates that systemic administration of SC-Exos to diabetic *db/db* mice with DPN significantly ameliorates DPN likely by increasing IENFs and reducing axonal and myelin damage of the sciatic nerve. Interactions between SC-Exo cargo miRs and their putative target proteins in sciatic nerves tissues may contribute to underlying molecular mechanisms mediating the SC-Exo therapy. These novel findings provide evidence that SC-Exos are effective for the treatment of DPN in mice.

In addition to myelination, Schwann cells release numerous factors and communicate with axons to regulate peripheral nerve function (4,5,18). Dysfunction of this communication is involved in the development of DPN (1,6,7). Exosomes play essential roles in intercellular communication by transferring their cargo between source and recipient cells (15,16). We previously showed that exosomes derived from HG-stimulated Schwann cells facilitate the development of DPN by reduction of epidermal nerve fibers in diabetic *db/db* mice (17). The current study demonstrates that SC-Exos have a potent therapeutic effect on DPN in the mouse. Although not excluding the possibility that other cell sources for exosomes may have a therapeutic effect for DPN, the observed therapeutic effect is somewhat specific because FC-Exos do not have any therapeutic effect on DPN. Using a rat model of sciatic nerve injury, Lopez-Verrilli et al. (18) reported that the administration of exosomes derived from healthy differentiated Schwann cells substantially enhances the regeneration of injured axons. Moreover, exosomes derived from human Schwann cells have a protective effect on DRG neurons injured by mechanical strain (39).

DPN involves large and small nerve fibers as well as myelinated and nonmyelinated nerve fibers. Reduction of

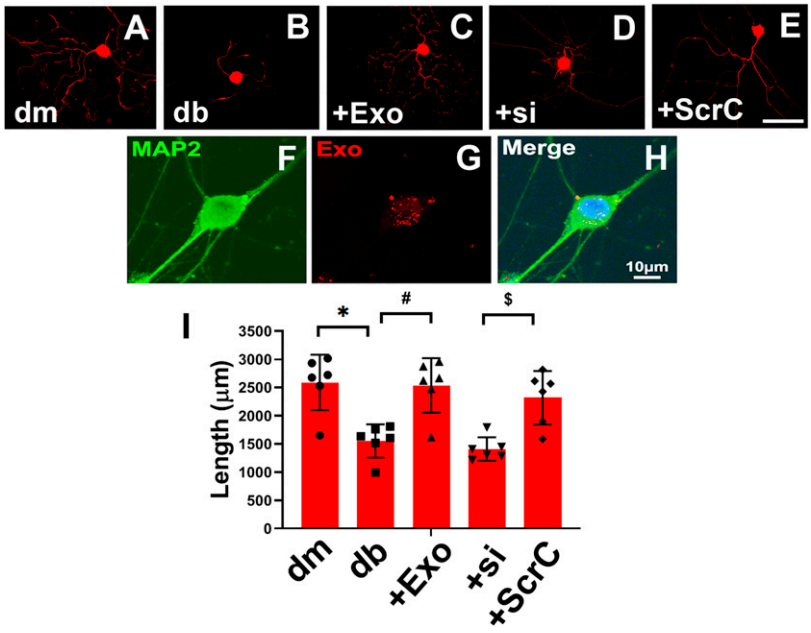

Figure 6—SC-Exos are internalized by DRG neurons and increase neurite outgrowth. Representative images of NFH-positive neurite of DRG neurons derived from nondiabetic mice (dm) (*A*), diabetic mice (db) (*B*), db mice treated with SC-Exos (+Exo) (*C*), and SC-Exo with reduced miR-27a (+si) (*D*) or scrambled control (+ScrC) (*E*). Scale bar in $E = 100$ μm. Representative confocal image of fluorescently Exo-fect-labeled SC-Exo (red) diffused within the cytoplasm of a MAP2-positive DRG neuron (green) (*F–H*). Quantitative data of neurite length of DRG neuron under different culture conditions (*I*). $n = 6$/group. *$P < 0.05$ vs. the dm DRG neurons; #$P < 0.05$ vs. the db DRG neurons; \$$P < 0.05$ vs. +ScrC.

IENFs induces dysfunction of small nerve fibers that respond to impairment of mechanical and thermal stimulations, the earliest distal symptoms of DPN (1,40). Clinically, reduction of IENFs in skin biopsy has been widely used as a reliable assay to evaluate DPN (3). Nerve conduction measurements assess large myelinated fiber function and have been used in patients as a standard procedure to diagnose DPN (41). Data from the current study indicate that SC-Exos improve IENFs, myelination, and NCVs and in concert, improve sensory nerve function and ameliorate neuropathic symptoms of DPN. However, we do not know whether the therapeutic effect of SC-Exos results from slowing and/or reversing damaged peripheral nerve function. We and others have demonstrated that diabetic *db/db* mice progressively develop impairments of small and large nerve fibers at age 20–28 weeks (12,42). Treatment of *db/db* mice with sildenafil has a more robust therapeutic effect in the early stage of DPN than in advanced DPN (25,43). Ultrastructural data in the current study showed signs of remyelination, suggesting a myelin repair process. We thus speculate that SC-Exos act on protecting and/or reversing damaged peripheral nerve fibers. Additional studies evaluating the temporal windows of SC-Exo treatment of DPN are warranted.

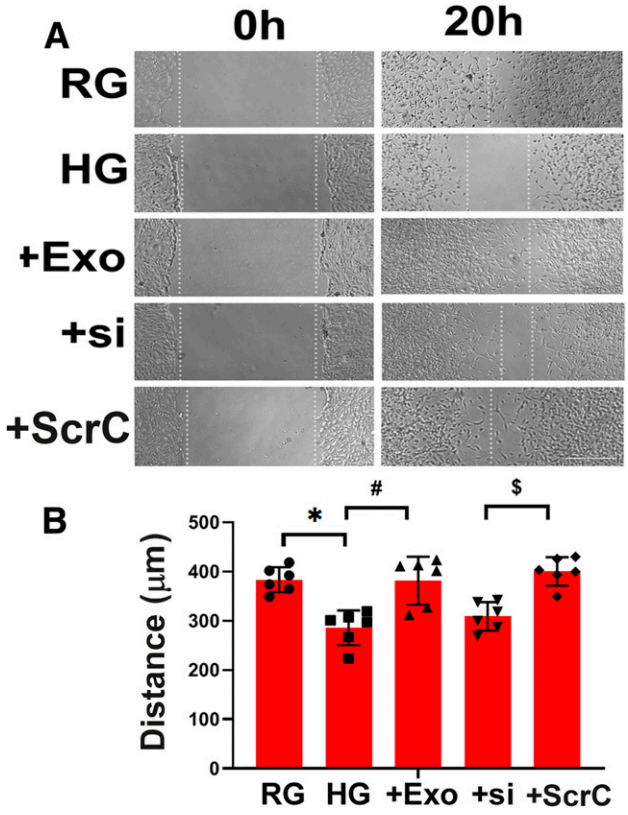

Figure 7—SC-Exos reverse HG-impaired Schwann cell migration. Representative images of migration of Schwann cells treated with RG, HG with or without SC-Exos (+Exo), SC-Exo with reduced miR-27a (+si), or scrambled control (+ScrC) (*A*). Quantitative data of migration of Schwann cells under different culture conditions (*B*). Scale bar = 100 μm. $n = 6$/group. *$P < 0.05$ vs. RG group; #$P < 0.05$ vs. HG group.

The SC-Exo treatment did not significantly alter blood glucose levels, suggesting that the therapeutic effect is not through reducing blood glucose levels. Diabetes-induced down- and upregulated miRs mediate the development of DPN (9,10,12,17). For example, diabetes-upregulated miRs, including miR-28, -31, and -130, in Schwann cells are detrimental to DPN by downregulating proteins that support axonal structures and function (17). The current study finds that diabetes substantially reduced miR-21, -27a, and -146a levels in the sciatic nerve tissue, which is consistent with reports from human and animal studies (12,14,33). Patients with T2D exhibit increased susceptibility to neuropathy when they have polymorphisms in miR-146a, miR-27a, and miR-124a genes (11). Mice with DPN exhibit significant reduction of let-7i and miR-27a (13). Elevation of let-7i and miR-146a by exogenous miR mimics substantially ameliorates DPN in mouse models of diabetes (12,14). The current study suggests that SC-Exo miRs interact with their putative proteins in recipient sciatic nerves of DRG neurons and Schwann cells. Compared with FC-Exos, SC-Exos were enriched with miR-21, -27a, and -146a, whereas SC-Exos with ablation of miR-27a lost the exosomal effect on promoting axonal growth of diabetic DRG neurons and migration of Schwann cells compared with naive SC-Exos. Moreover, our in vivo data indicate that intravenously administered SC-Exos were associated with elevation and reduction of diabetes-decreased miR-21, -27a, and -146a and augmented proteins of SEMA6A, RhoA, PTEN, and NF-κB in the sciatic nerve tissue, respectively. Bioinformatics analysis predicted that these three miRs could either directly or indirectly target SEMA6A, RhoA, PTEN, and NF-κB genes, and these proteins have been demonstrated to damage axons and inhibit axonal growth (37,44–46). In addition to proteins in the extracellular matrix to inhibit axonal growth, emerging data indicate that endogenous proteins within neurons and axons play major roles in blocking axonal growth after axonal injury (44). These endogenous axonal inhibitory proteins include PTEN and RhoA (45,47,48). Knockdown of PTEN in DRG neurons promotes myelinated axonal regrowth and skin re-enervation in diabetic mice (47), while blockage of the RhoA/ROCK (Rho-associated kinase) signaling pathway enhances axonal regeneration and relieves pain in DPN (45). In addition, treatment of diabetic *db/db* mice with miR-146a mimics augmented small and large nerve fibers by inactivation of NF-κB through targeting IRAK1 and TRAF6 genes in Schwann cells and axons of DRG neurons (12). The current study provides evidence that intravenously administered SC-Exos are internalized by MBP-positive Schwann cells and NFH-positive nerve fibers in sciatic nerves, as demonstrated by immunofluorescent staining, and are internalized by neurofilaments and mitochondria of sciatic nerves as shown by TEM. Together, our data along with others suggest that the interaction of SC-Exo

miRs with their target genes in recipient axons and Schwann cells may underlie mechanisms facilitating the therapeutic effect of SC-Exos on DPN. However, it remains unknown whether increased miRs in the sciatic nerve tissue are caused by directly transferring exosomal cargo miRs to recipients and/or by upregulating recipient cell miRs triggered by SC-Exo miRs. Additionally, the current study cannot exclude the possibility that other miRs within SC-Exos and exosomal cargo proteins, such as HSP70, may also contribute the observed therapeutic effect.

Abnormal liver function and dyslipidemia are associated with DPN (49). A recent study in patients with T2D and DPN suggested that reduction of serum cholesterol levels exacerbates neuropathy (50). Our data showed that SC-Exos did not significantly change total cholesterol levels. However, we cannot exclude an effect of SC-Exos on dyslipidemia and liver function, and further investigations in this area are warranted. Nevertheless, the current study suggests that SC-Exos represent a novel therapeutic approach for the treatment of DPN.

Acknowledgments. The authors thank Meser M. Ali (Department of Neurosurgery, Henry Ford Hospital), Julie Landschoot-Ward (Department of Neurology, Henry Ford Hospital), Amy Kemper (Department of Pathology, Henry Ford Hospital), Qing-e Lu (Department of Neurology, Henry Ford Hospital), and Supata Santra (Department of Neurology, Henry Ford Hospital) for technical assistance.

Funding. This work was supported by the National Institutes of Health National Institute of Neurological Disorders and Stroke RO1-NS-075084 (to L.W.) and National Institute of Diabetes and Digestive and Kidney Diseases RO1-DK-097519 (to L.W.) and IR56-DK-115601 (to L.W.).

Duality of Interest. No potential conflicts of interest relevant to this article were reported.

Author Contributions. L.W., M.C., and Z.G.Z. designed the study. L.W., A.S., X.L., and M.L. analyzed data. L.W. and Z.G.Z. wrote the manuscript. M.C. reviewed and edited the manuscript. A.S., X.L., Y.Z., X.W., and P.C. performed experiments. All authors read and approved the final version of the manuscript. L.W. is the guarantor of this work and, as such, had full access to all the data in the study and takes responsibility for the integrity of the data and the accuracy of the data analysis.

References

1. Feldman EL, Nave KA, Jensen TS, Bennett DLH. New horizons in diabetic neuropathy: mechanisms, bioenergetics, and pain. Neuron 2017;93:1296–1313
2. Boucek P. Advanced diabetic neuropathy: a point of no return? Rev Diabet Stud 2006;3:143–150
3. Tesfaye S, Boulton AJ, Dyck PJ, et al.; Toronto Diabetic Neuropathy Expert Group. Diabetic neuropathies: update on definitions, diagnostic criteria, estimation of severity, and treatments. Diabetes Care 2010;33:2285–2293
4. Lehmann HC, Höke A. Schwann cells as a therapeutic target for peripheral neuropathies. CNS Neurol Disord Drug Targets 2010;9:801–806
5. Corfas G, Velardez MO, Ko CP, Ratner N, Peles E. Mechanisms and roles of axon-Schwann cell interactions. J Neurosci 2004;24:9250–9260
6. Gonçalves NP, Vægter CB, Andersen H, Østergaard L, Calcutt NA, Jensen TS. Schwann cell interactions with axons and microvessels in diabetic neuropathy. Nat Rev Neurol 2017;13:135–147
7. Eckersley L. Role of the Schwann cell in diabetic neuropathy. Int Rev Neurobiol 2002;50:293–321
8. Lorenzen J, Kumarswamy R, Dangwal S, Thum T. MicroRNAs in diabetes and diabetes-associated complications. RNA Biol 2012;9:820–827
9. Xourgia E, Papazafiropoulou A, Melidonis A. Circulating microRNAs as biomarkers for diabetic neuropathy: a novel approach. World J Exp Med 2018;8:18–23
10. Moura J, Børsheim E, Carvalho E. The role of microRNAs in diabetic complications-special emphasis on wound healing. Genes (Basel) 2014;5:926–956
11. Wang TT, Chen YJ, Sun LL, Zhang SJ, Zhou ZY, Qiao H. Affection of single-nucleotide polymorphisms in miR-27a, miR-124a, and miR-146a on susceptibility to type 2 diabetes mellitus in Chinese Han people. Chin Med J (Engl) 2015;128:533–539
12. Liu XS, Fan B, Szalad A, et al. MicroRNA-146a mimics reduce the peripheral neuropathy in type 2 diabetic mice. Diabetes 2017;66:3111–3121
13. Kobayashi M, Zochodne DW. Diabetic neuropathy and the sensory neuron: new aspects of pathogenesis and their treatment implications. J Diabetes Investig 2018;9:1239–1254
14. Cheng C, Kobayashi M, Martinez JA, et al. Evidence for epigenetic regulation of gene expression and function in chronic experimental diabetic neuropathy. J Neuropathol Exp Neurol 2015;74:804–817
15. Lai CP, Breakefield XO. Role of exosomes/microvesicles in the nervous system and use in emerging therapies. Front Physiol 2012;3:228
16. Schneider A, Simons M. Exosomes: vesicular carriers for intercellular communication in neurodegenerative disorders. Cell Tissue Res 2013;352:33–47
17. Jia L, Chopp M, Wang L, Lu X, Szalad A, Zhang ZG. Exosomes derived from high-glucose-stimulated Schwann cells promote development of diabetic peripheral neuropathy. FASEB J 2018;32:6911–6922
18. Lopez-Verrilli MA, Picou F, Court FA. Schwann cell-derived exosomes enhance axonal regeneration in the peripheral nervous system. Glia 2013;61:1795–1806
19. Xin H, Li Y, Buller B, et al. Exosome-mediated transfer of miR-133b from multipotent mesenchymal stromal cells to neural cells contributes to neurite outgrowth. Stem Cells 2012;30:1556–1564
20. Zhang Y, Chopp M, Liu XS, et al. Exosomes derived from mesenchymal stromal cells promote axonal growth of cortical neurons. Mol Neurobiol 2017;54:2659–2673
21. Xin H, Katakowski M, Wang F, et al. MicroRNA cluster miR-17-92 cluster in exosomes enhance neuroplasticity and functional recovery after stroke in rats. Stroke 2017;48:747–753
22. Ekanger LA, Ali MM, Allen MJ. Oxidation-responsive Eu(2+/3+)-liposomal contrast agent for dual-mode magnetic resonance imaging. Chem Commun (Camb) 2014;50:14835–14838
23. Xin H, Wang F, Li Y, et al. Secondary release of exosomes from astrocytes contributes to the increase in neural plasticity and improvement of functional recovery after stroke in rats treated with exosomes harvested from microRNA 133b-overexpressing multipotent mesenchymal stromal cells. Cell Transplant 2017;26:243–257
24. Ii M, Nishimura H, Kusano KF, et al. Neuronal nitric oxide synthase mediates statin-induced restoration of vasa nervorum and reversal of diabetic neuropathy. Circulation 2005;112:93–102
25. Wang L, Chopp M, Szalad A, et al. Sildenafil ameliorates long term peripheral neuropathy in type II diabetic mice. PLoS One 2015;10:e0118134
26. Wang L, Chopp M, Jia L, et al. Therapeutic benefit of extended thymosin β4 treatment is independent of blood glucose level in mice with diabetic peripheral neuropathy. J Diabetes Res 2015;2015:173656
27. Dixon WJ. Efficient analysis of experimental observations. Annu Rev Pharmacol Toxicol 1980;20:441–462
28. Chaplan SR, Bach FW, Pogrel JW, Chung JM, Yaksh TL. Quantitative assessment of tactile allodynia in the rat paw. J Neurosci Methods 1994;53:55–63

29. Di Scipio F, Raimondo S, Tos P, Geuna S. A simple protocol for paraffin-embedded myelin sheath staining with osmium tetroxide for light microscope observation. Microsc Res Tech 2008;71:497–502
30. Zhang Z, Zhang RL, Jiang Q, Raman SB, Cantwell L, Chopp M. A new rat model of thrombotic focal cerebral ischemia. J Cereb Blood Flow Metab 1997;17:123–135
31. Liu XS, Chopp M, Pan WL, et al. MicroRNA-146a promotes oligodendrogenesis in stroke. Mol Neurobiol 2017;54:227–237
32. Justus CR, Leffler N, Ruiz-Echevarria M, Yang LV. In vitro cell migration and invasion assays. J Vis Exp 2014;(88):e51046
33. Madhyastha R, Madhyastha H, Nakajima Y, Omura S, Maruyama M. MicroRNA signature in diabetic wound healing: promotive role of miR-21 in fibroblast migration. Int Wound J 2012;9:355–361
34. Tolkovsky AM. Is PTEN hyperactivity behind poor regeneration in diabetic neuropathy? Brain 2014;137:977–978
35. Ohsawa M, Ishikura K, Mutoh J, Hisa H. Involvement of inhibition of RhoA/Rho kinase signaling in simvastatin-induced amelioration of neuropathic pain. Neuroscience 2016;333:204–213
36. Ohsawa M, Kamei J. RhoA/Rho kinase signaling in the spinal cord and diabetic painful neuropathy. Eur J Pharmacol 2010;644:1–4
37. Xu XM, Fisher DA, Zhou L, et al. The transmembrane protein semaphorin 6A repels embryonic sympathetic axons. J Neurosci 2000;20:2638–2648
38. Mauti O, Domanitskaya E, Andermatt I, Sadhu R, Stoeckli ET. Semaphorin6A acts as a gate keeper between the central and the peripheral nervous system. Neural Dev 2007;2:28
39. Zhou M, Hu M, He S, et al. Effects of RSC96 Schwann cell-derived exosomes on proliferation, senescence, and apoptosis of dorsal root ganglion cells in vitro. Med Sci Monit 2018;24:7841–7849
40. Lauria G, Devigili G. Skin biopsy as a diagnostic tool in peripheral neuropathy. Nat Clin Pract Neurol 2007;3:546–557
41. Jin HY, Park TS. Can nerve conduction studies detect earlier and predict clinical diabetic neuropathy? J Diabetes Investig 2015;6:18–20
42. Sullivan KA, Hayes JM, Wiggin TD, et al. Mouse models of diabetic neuropathy. Neurobiol Dis 2007;28:276–285
43. Wang L, Chopp M, Szalad A, et al. Phosphodiesterase-5 is a therapeutic target for peripheral neuropathy in diabetic mice. Neuroscience 2011;193:399–410
44. Christie KJ, Webber CA, Martinez JA, Singh B, Zochodne DW. PTEN inhibition to facilitate intrinsic regenerative outgrowth of adult peripheral axons. J Neurosci 2010;30:9306–9315
45. Hiraga A, Kuwabara S, Doya H, et al. Rho-kinase inhibition enhances axonal regeneration after peripheral nerve injury. J Peripher Nerv Syst 2006;11:217–224
46. Mattson MP, Camandola S. NF-kappaB in neuronal plasticity and neurodegenerative disorders. J Clin Invest 2001;107:247–254
47. Singh B, Singh V, Krishnan A, et al. Regeneration of diabetic axons is enhanced by selective knockdown of the PTEN gene. Brain 2014;137:1051–1067
48. Cheng C, Singh V, Krishnan A, Kan M, Martinez JA, Zochodne DW. Loss of innervation and axon plasticity accompanies impaired diabetic wound healing. PLoS One 2013;8:e75877
49. Yorek MA. The potential role of fatty acids in treating diabetic neuropathy. Curr Diab Rep 2018;18:86
50. Jende JME, Groener JB, Rother C, et al. Association of serum cholesterol levels with peripheral nerve damage in patients with type 2 diabetes. JAMA Netw Open 2019;2:e194798